AIMS Mathematics, 9(3): 6648–6667.
DOI: 10.3934/math.2024324
Received: 17 November 2023
Revised: 21 December 2023
Accepted: 10 January 2024
Published: 06 February 2024

https://www.aimspress.com/journal/Math

Research article

Local convergence study of tenth-order iterative method in Banach spaces with basin of attraction

Kasmita Devi and Prashanth Maroju*

Department of Mathematics, SAS, VIT-AP University, Amaravati, 522237, Andhra Pradesh, India

* **Correspondence:** Email: maroju.prashanth@gmail.com; Tel: +8309592957.

Abstract: Many applications from computational mathematics can be identified for a system of non-linear equations in more generalized Banach spaces. Analytical methods do not exist for solving these type of equations, and so we solve these equations using iterative methods. We introduced a new numerical technique for finding the roots of non-linear equations in Banach space. The method is tenth-order and it is an extension of the fifth-order method which is developed by Arroyo et.al. [1]. We provided a convergence analysis to demonstrate that the method exhibits tenth-order convergence. Also, we discussed the local convergence properties of the suggested method which depends on the fundamental supposition that the first-order Fréchet derivative of the involved function Υ satisfies the Lipschitz conditions. This new approach is not only an extension of prior research, but also establishes a theoretical concept of the radius of convergence. We validated the efficacy of our method through various numerical examples. Our method is comparable with the methods of Tao Y et al. [2]. We also compared it with higher-order iterative methods, and we observed that it either performs similarly or better for the numerical examples. We also gave the basin of attraction to demonstrate the behaviour in the complex plane.

Keywords: local convergence; Lipschitz continuity; Fréchet derivative; non-linear equations
Mathematics Subject Classification: 65Hxx, 65H05, 65H10

1. Introduction

In the realm of scientific and engineering applications, many problems often lead to the formulation of nonlinear equations that resist straightforward analytical solutions. These equations, encompassing a wide range of complexities, arise in various fields such as biology, economics, engineering, and physics. While linear equations can be tackled through well-established methods, nonlinear equations necessitate more sophisticated techniques. Among these, iterative methods play a pivotal role in approximating solutions.

Iterative methods involve the process of repeatedly refining an initial estimate to converge towards the true solution of an equation. These methods find extensive usage in both linear and nonlinear scenarios. When it comes to nonlinear equations, they provide a powerful tool kit for solving equations that do not involve derivatives. In particular, higher-order iterative methods bring for a class of techniques capable of yielding accurate solutions for nonlinear non-differential equations of various orders.

One crucial aspect of numerical analysis is understanding the behavior and performance of numerical methods, especially in the context of iterative techniques used to solve nonlinear equations. Local convergence analysis [1,3–6] is a fundamental tool in assessing the behavior of iterative methods in the vicinity of a potential solution. When dealing with iterative methods, it is important to consider not only whether the method converges, i.e. approaches a solution, but also how quickly and reliably it converges. Local convergence analysis specifically examines the behavior of an iterative method when starting from an initial guess that is close to the true solution. In local convergence analysis, the convergence behavior is often characterized by a convergence radius. This radius defines a region around the true solution within which the iterative method is expected to converge. If the initial guess falls within this region, the method is likely to converge to the solution.

Many researchers have developed a higher-order iterative methods for the solution of nonlinear equations [7–11]. One of the most demanding iterative methods is Newton-Rapshon method denoted which has second order of convergence. The Halley and Chebyshev methods third order of convergence [12]. Fourth-order convergence developed by [12–15]. In [7, 16, 17] the reserachers developed fifth-order convergence. In [18, 19] the reserachers developed sixth-order convergence. Eighth-order convergence analysis was discussed by [2, 14].

The main motive of this paper is to develop a higher tenth-order iterative technique by extending the fifth-order method proposed by Arroyo and Cordero [1] for finding the roots of nonlinear equations in Banach space. In our research, we analyze how well our proposed method works within a specific region, focusing on the behavior of its first Fréchet derivative and Lipschitz constants. We also determine the range within which our method is effective and provide ways to estimate errors in the distances $\|\chi_n - \chi^*\|$. We solved various numerical problems using Mathematica 11.3 in order to demonstrate the efficacy of the methods. The results of the proposed methods are compared with the results of the Tao and Madhu [2]. The proposed technique represented in the complex plane by using the basin of attraction.

This paper is organized as follows: In Section 2, we have given the proposed tenth-order iterative technique. In Section 3, we have derived the convergence analysis of proposed technique. In Section 4, we proved the local convergence analysis of our method. In Section 5, we gave some numerical examples to verify the results obtained in Section 2. In Section 6, we studied the basin of attraction of the proposed iterative method. Finally, in Section 7, we have given the conclusion.

2. Proposed method

In this section, we developed our tenth-order iterative method using the fifth-order method.

In 2015, Arroyo and Cordero [1] developed the fifth-order iterative method as follows:

$$\begin{aligned} \psi_n &= \chi_n - [\Upsilon'(\chi_n)]^{-1}\Upsilon(\chi_n), \\ z_n &= \psi_n - 5[\Upsilon'(\chi_n)]^{-1}\Upsilon(\psi_n), \\ \chi_{n+1} &= z_n - \frac{1}{5}[\Upsilon'(\chi_n)]^{-1}[-16\Upsilon(\psi_n) + \Upsilon(z_n)]. \end{aligned} \tag{2.1}$$

We have generalized (2.1) by adding the 4th step as follows:

$$\begin{aligned} \psi_n &= \chi_n - [\Upsilon'(\chi_n)]^{-1}\Upsilon(\chi_n), \\ z_n &= \psi_n - 5[\Upsilon'(\chi_n)]^{-1}\Upsilon(\psi_n), \\ w_{n+1} &= z_n - \frac{1}{5}[\Upsilon'(\chi_n)]^{-1}[-16\Upsilon(\psi_n) + \Upsilon(z_n)], \\ \chi_{n+1} &= w_n - [\Upsilon'(w_n)]^{-1}(\Upsilon(w_n)). \end{aligned} \tag{2.2}$$

Now, we discuss the convergence analysis of our proposed method.

3. Convergence analysis

Theorem 3.1. *Assume we have a function Υ defined on an open interval Ω, with a simple root χ^* within that interval. If $\Upsilon(\chi)$ is smooth in the vicinity of the root χ^*, we can employ the methods described by* (2.2)*, which have a high accuracy, specifically being of order 10 and satisfying the following error equation:*

$$e_{n+1} = 4c_2^5(7c_2^2 + 2c_3)^2 e_5^{10} + O(e_5^{11}). \tag{3.1}$$

Proof. Let $e_n = \chi_n - \chi^*$ be the error in nth iteration. Using Taylor's series expansion around χ^*, we get

$$\begin{aligned} \Upsilon(\chi_n) &= \Upsilon(\chi^*) + \frac{\Upsilon'(\chi^*)}{1!}(\chi_n - \chi^*) + \frac{\Upsilon''(\chi^*)}{2!}(\chi_n - \chi^*)^2 + \frac{\Upsilon'''(\chi^*)}{3!}(\chi_n - \chi^*)^3 + \cdots, \\ \Upsilon(\chi_n) &= \Upsilon'(\chi^*)\Big[e_n + c_2e_n^2 + c_2e_n^3 + c_3e_n^4 + c_4e_n^4 + c_5e_n^5 + c_6e_n^6 + c_7e_n^7 \cdots\Big], \\ \Upsilon'(\chi_n) &= \Upsilon'(\chi^*)\Big[1 + 2c_2e_n + 3c_2e_n^2 + 4c_3e_n^3 + 4c_4e_n^3 + 5c_5e_n^4 + c_6e_n^5 + c_7e_n^6 \cdots\Big]. \end{aligned}$$

From the first step of (2.2), we get

$$\begin{aligned} \psi_n =& c_2e_n^2 + \left(2c_3 - 2c_2^2\right)e_n^3 + \left(4c_2^3 - 7c_3c_2 + 3c_4\right)e_n^4 + \left(-8c_2^4 + 20c_3c_2^2 - 10c_4c_2 - 6c_3^2 + 4c_5\right)e_n^5 \\ &+ \left(16c_2^5 - 52c_3c_2^3 + 28c_4c_2^2 + \left(33c_3^2 - 13c_5\right)c_2 - 17c_3c_4 + 5c_6\right)e_n^6 \\ &- 2\left(16c_2^6 - 64c_3c_2^4 + 36c_4c_2^3 + 9\left(7c_3^2 - 2c_5\right)c_2^2 + (8c_6 - 46c_3c_4)c_2 - 9c_3^3 + 6c_4^2 + 11c_3c_5\right)e_n^7 + \cdots, \end{aligned}$$

From the second step of (2.2), we get

$$\begin{aligned} z_n =& -4c_2e_n^2 + \left(18c_2^2 - 8c_3\right)e_n^3 + \left(-61c_2^3 + 63c_3c_2 - 12c_4\right)e_n^4 \\ &+ 2\left(91c_2^4 - 150c_3c_2^2 + 45c_4c_2 + 27c_3^2 - 8c_5\right)e_n^5 \\ &+ \left(-504c_2^5 + 1148c_3c_2^3 - 422c_4c_2^2 + \left(117c_5 - 482c_3^2\right)c_2 + 153c_3c_4 - 20c_6\right)e_n^6 \\ &+ 2(664c_2^6 - 1936c_3c_2^4 + 804c_4c_2^3 + 4\left(333c_3^2 - 68c_5\right)c_2^2 \end{aligned}$$

$$+ (72c_6 - 674c_3c_4)\, c_2 - 126c_3^3 + 54c_4^2 + 99c_3c_5)e_n^7 + \cdots .$$

From the third step of (2.2), we get

$$w_n = \left(14c_2^4 + 4c_3c_2^2\right)e_n^5 + c_2\left(-140c_2^4 + 65c_3c_2^2 + 4c_4c_2 + 17c_3^2\right)e_n^6 + 2\left(430c_2^6 - 535c_3c_2^4 + 44c_4c_2^3 + \left(37c_3^2 + 2c_5\right)c_2^2 + 22c_3c_4c_2 + 9c_3^3\right)e_n^7 + \cdots .$$

Finally, we get

$$e_{n+1} = 4c_2^5\left(7c_2^2 + 2c_3\right)^2 e_n^{10} + O\left(e_n^{11}\right). \tag{3.2}$$

Equation (3.2) shows that the order of convergence of (2.2) is tenth-order.

This completes the proof. □

4. Local convergence

In this section, we discuss the local convergence of (2.2) in Banach space.

Theorem 4.1. *Let, $\Upsilon : \Omega \subset S \to S$ be a differentiable function. Suppose that there exists $\chi^* \in \Omega$, given parameters $\lambda_0 > 0, \lambda > 0, M \geq 1$, and for each $\chi, \psi \in \Omega$ the following are true:*

$$\Upsilon(\chi^*) = 0, (\Upsilon'(\chi^*))^{-1} \in L(S, S),$$

$$\left\|\Upsilon'(\chi^*)^{-1}(\Upsilon'(\chi) - \Upsilon'(\chi^*))\right\| \leq \lambda_0\|\chi - \chi^*\|, \tag{4.1}$$

$$\left\|\Upsilon'(\chi^*)^{-1}(\Upsilon'(\chi) - \Upsilon'(\psi)\right\| \leq \lambda\|\chi - \psi\|, \tag{4.2}$$

$$\left\|\Upsilon'(\chi^*)^{-1}(\Upsilon'(\chi)\right\| \leq M, \tag{4.3}$$

$$\overline{U}(\chi^*, r) \subseteq \Omega. \tag{4.4}$$

Then, the sequence generated by method (2.2) *for $\chi_0 \in U(\chi^*, r) \setminus \chi^*$ is well defined in $\overline{U}(\chi^*, r)$ for each $n = 0, 1, 2, 3, ...$ and converges to χ^*. Moreover the following estimates hold.*

$$\|\psi_n - \chi^*\| \leq \tau_1(\|\chi_n - \chi^*\|)\|\chi_n - \chi^*\| < \|\chi_n - \chi^*\| < 1, \tag{4.5}$$

$$\|z_n - \chi^*\| \leq \tau_2(\|\chi_n - \chi^*\|)\|\chi_n - \chi^*\| < \|\chi_n - \chi^*\| < 1, \tag{4.6}$$

$$\|w_n - \chi^*\| \leq \tau_3(\|\chi_n - \chi^*\|)\|\chi_n - \chi^*\| < \|\chi_n - \chi^*\| < 1, \tag{4.7}$$

$$\|\chi_{n+1} - \chi^*\| \leq \tau_4(\|\chi_n - \chi^*\|)\|\chi_n - \chi^*\| < \|\chi_n - \chi^*\| < 1. \tag{4.8}$$

Furthermore, suppose that there exists$R \in [r, \frac{2}{\lambda_0})$ such that $\overline{U}(\chi^*, R)$. Then, the limit point χ^* is the only solution of $\Upsilon(\chi) = 0$ in $\overline{U}(\chi^*, R)$.

Proof. In this section, we present the local convergence analysis of our developed iterative method (2.2). Let $\lambda_0 > 0$, $L > 0$, $M > 0$ be the given parameters. Suppose, there exists $\chi^* \in \Omega$ such that $\Upsilon(\chi^*) = 0$. Let us assume that

$$\left\|\Upsilon'(\chi^*)^{-1}(\Upsilon'(\chi) - \Upsilon'(\chi^*))\right\| \leq \lambda_0\|\chi - \chi^*\|.$$

Since $\chi_0 \in D$,

$$\left\|\Upsilon'(\chi^*)^{-1}(\Upsilon'(\chi_0) - \Upsilon'(\chi^*))\right\| \leq \lambda_0\|\chi_0 - \chi^*\|. \tag{4.9}$$

Let us assume that $\|\chi_0 - \chi^*\| < \frac{1}{\lambda_0}$, which implies

$$\left\|\Upsilon'(\chi^*)^{-1}\Upsilon'(\chi_0) - I\right\| < 1,$$

$(\Upsilon'(\chi_0))^{-1} \in L(S, S)$, and the value of $\left\|(\Upsilon'(\chi_0))^{-1}\right\|$ is

$$\left\|(\Upsilon'(\chi_0))^{-1}\Upsilon'(\chi)^*\right\| = \frac{1}{1 - \lambda_0\|\chi_0 - \chi^*\|}. \tag{4.10}$$

From the first step of (2.2),

$$\psi_n = \chi_n - (\Upsilon'(\chi_n))^{-1}\Upsilon(\chi_n). \tag{4.11}$$

Putting $n = 0$ in (4.11),

$$\psi_0 = \chi_0 - (\Upsilon'(\chi_0))^{-1}\Upsilon(\chi_0),$$

$$\psi_0 - \chi^* = -(\Upsilon'(\chi_0))^{-1}\int_0^1 [\Upsilon'(\chi^* + \theta(\chi_0 - \chi^*)) - \Upsilon'(\chi_0)]\, d\theta(\chi_0 - \chi^*).$$

Taking the norm on both sides, we get

$$\|\psi_0 - \chi^*\| = \left\|(\Upsilon'(\chi_0))^{-1}\int_0^1 [\Upsilon'(\chi^* + \theta(\chi_0 - \chi^*)) - \Upsilon'(\chi_0)]\, d\theta(\chi_0 - \chi^*)\right\|,$$

$$\|\psi_0 - \chi^*\| \leq \left\|(\Upsilon'(\chi_0))^{-1}\Upsilon'(\chi^*)\int_0^1 (\Upsilon'(\chi^*))^{-1}\Big[\Upsilon'(\chi^* + \theta(\chi_0 - \chi^*)) - \Upsilon'(\chi_0)\ d\theta\Big]\right\|\|\chi_0 - \chi^*\|,$$

$$\|\psi_0 - \chi^*\| \leq \frac{\lambda\|\chi_0 - \chi^*\|^2}{2(1 - \lambda_0\|\chi_0 - \chi^*\|)},$$

$$\|\psi_0 - \chi^*\| \leq \tau_1\|\chi_0 - \chi^*\|\,\|\chi_0 - \chi^*\|,$$

for $n = 0$, $\psi_0 \in U(\chi^*, r)$,

$$\tau_1(t) = \frac{\lambda t}{2(1 - \lambda_0 t)}. \tag{4.12}$$

From the second step of (2.2), we get

$$z_0 = \psi_0 - 5[\Upsilon'(\chi_0)]^{-1}\Upsilon(\psi_0).$$

Taking the norm on both sides, we get

$$\|z_0 - \chi^*\| = \left\|(\psi_0 - \chi^*) - 5[\Upsilon'(\chi_0)]^{-1}\Upsilon(\psi_0)\right\|,$$

$$\begin{aligned}
\|z_0 - \chi^*\| &\leq \|\psi_0 - \chi^*\| + 5\left\|\Upsilon(\psi_0)[\Upsilon'(\chi_0)]^{-1}\right\| \\
&\leq \|\psi_0 - \chi^*\| + 5M\|\psi_0 - \chi^*\|\frac{1}{1 - \lambda_0\|\chi_0 - \chi^*\|} \\
&= \|\psi_0 - \chi^*\| + \left[1 + \frac{5M}{1 - \lambda_0\|\chi_0 - \chi^*\|}\right] \\
&\leq \tau_1\|\chi_0 - \chi^*\| + \left[1 + \frac{5M}{1 - \lambda_0\|\chi_0 - \chi^*\|}\right]\|\chi_0 - \chi^*\| \\
&= \tau_2\left(\|\chi_0 - \chi^*\|\right)\|\chi_0 - \chi^*\| \\
&< r.
\end{aligned}$$

Since $\|z_0 - \chi_0\| < r$, then $z_0 \in U(\chi^*, r)$, where

$$\tau_2(t) = \tau_1(t)\Big[1 + \frac{5M}{1 - \lambda_0 t}\Big]. \tag{4.13}$$

From the third step of (2.2), we get

$$w_{n+1} = z_n - \frac{1}{5}[\Upsilon'(\chi_n]^{-1}[-16\Upsilon(\psi_n) + \Upsilon(z_n)]. \tag{4.14}$$

Taking the norm on both sides, we get

$$\begin{aligned}
\|w_0 - \chi_0\| &\leq \|z_0 - \chi_0\| + \frac{16}{5}\Big\|\Upsilon(\psi_0)(\Upsilon'(\chi_0))^{-1}\Big\| + \frac{1}{5}\Big\|\Upsilon(z_0)(\Upsilon'(\chi_0))^{-1}\Big\| \\
&\leq \|z_0 - \chi_0\| + \frac{16}{5}M\|\psi_0 - \chi^*\|\frac{1}{1 - \lambda_0\|\chi_0 - \chi^*\|} \\
&\quad + \frac{1}{5}M\|z_0 - \chi^*\|\frac{1}{1 - \lambda_0\|\chi_0 - \chi^*\|} \\
&\leq \tau_2(\|\chi_0 - \chi^*\|)\|\chi_0 - \chi^*\| \\
&\quad + \frac{16}{5}M\tau_1(\|\chi_0 - \chi^*\|)\|\chi_0 - \chi^*\|\frac{1}{1 - \lambda_0\|\chi_0 - \chi^*\|} \\
&\quad + \frac{1}{5}M\tau_2\|(\chi_0 - \chi^*)\|\|(\chi_0 - \chi^*)\|\frac{1}{1 - \lambda_0\|\chi_0 - \chi^*\|} \\
&= \Big(\tau_2\|(\chi_0 - \chi^*)\|\Big[1 + \frac{M}{5}\frac{1}{1 - \lambda_0\|\chi_0 - \chi^*\|}\Big] \\
&\quad + \frac{16}{5}M\tau_1(\|\chi_0 - \chi^*\|\frac{1}{1 - \lambda_0\|\chi_0 - \chi^*\|}\Big)\|\chi_0 - \chi^*\| \\
&\leq \tau_3(\|\chi_0 - \chi^*\|)\|\chi_0 - \chi^*\| \\
&< r,
\end{aligned}$$

where

$$\tau_3(t) = \tau_2(t)\Big[1 + \frac{M}{5(1 - \lambda_0 t)}\Big] + \frac{16}{5}M\tau_1(t)\frac{1}{1 - \lambda_0 t}. \tag{4.15}$$

From the final step of (2.2),

$$\chi_{n+1} = w_n - [\Upsilon'(w_n)]^{-1}(\Upsilon(w_n)).$$

Taking the norm on both sides, we get

$$\begin{aligned}
\|\chi_1 - \chi^*\| &= \Big\|w_0 - \chi^* - \Upsilon(w_0)(\Upsilon'(w_0))^{-1}\Big\| \\
&\leq \tau_3(\|\chi_0 - \chi^*\|)\|\chi_0 - \chi^*\| + M\|w_0 - \chi^*\|\frac{1}{1 - \lambda_0\|w_0 - \chi^*\|} \\
&\leq \tau_3(\|\chi_0 - \chi^*\|)\|\chi_0 - \chi^*\| \\
&\quad + M\tau_3(\|\chi_0 - \chi^*\|)\|\chi_0 - \chi^*\|\frac{1}{1 - \lambda_0\tau_3(\|\chi_0 - \chi^*\|)\|\chi_0 - \chi^*\|} \\
&= \left(\tau_3(\|\chi_0 - \chi^*\|)\Big[1 + M\frac{1}{1 - \lambda_0\tau_3(\|\chi_0 - \chi^*\|}\Big]\right)\|\chi_0 - \chi^*\| \\
&= \tau_4(\|\chi_0 - \chi^*\|)\|\chi_0 - \chi^*\| \\
&< r,
\end{aligned}$$

where

$$\tau_4(t) = \tau_3(t)\Big[1 + M\frac{1}{1-\lambda_0\tau_3(t)}\Big]. \tag{4.16}$$

From this, we can conclude that $\chi_1 \in U(\chi^*, r)$ for $n = 0$. By simply replacing $\chi_0, \psi_0, z_0, w_0, \chi_1$ as $\chi_k, \psi_k, z_k, w_k, \chi_{k+1}$ we get

$$\|\chi_{k+1} - \chi^*\| < \|\chi_k - \chi^*\| < r.$$

Since $\|\chi_{k+1} - \chi^*\| < r$, that means $\chi_{k+1} \in U(\chi^*, r)$.

Uniqueness: To show the uniqueness part, let ψ^* be another root. Then, by definition, $\Upsilon(\psi^*) = 0$ and $\psi^* \in \overline{U}(\chi^*, R)$.

Let $T = \int_0^1 \Upsilon'(\psi^* + \theta(\chi^* - \psi^*))d\theta$.

Now,

$$\begin{aligned}\left\|\Upsilon'(\chi^*)^{-1}(T - \Upsilon(\chi^*)\right\| &\leq \left\|\int_0^1 \lambda_0(\psi^* + \theta(\chi^* - \psi^*))d\theta\right\| \\ &< 1.\end{aligned} \tag{4.17}$$

By applying the Banach Inversion Lemma, T^{-1} exists. Hence, $\psi^* = \chi^*$.

This completes the proof. □

5. Numerical examples

In this section, we present a comprehensive numerical comparison between our newly developed tenth-order iterative method and the existing higher-order iterative method [2]. We demonstrate the performance of the methods. All experiments were conducted on Mathematica 11.3.

5.1. Real-world problems

Example 5.1. *(Classical projectile problem) [2] Suppose someone is standing on a tower and want to launch an object (like a ball) off the tower at a certain speed and angle so that it reaches a hill in the distance. The hill is represented by a function which tells us its height at any horizontal distance. To figure out the best angle to launch the object (the projectile) so that it travels the farthest horizontally and hits the hill, we need the following:*

- *The height of the tower= h;*
- *The initial speed of launching an object = v;*
- *From the horizontal the angle = θ;*
- *There's a hill in the distance described by a function=w(χ);*
- *The height of the hill at any horizontal distance=χ.*

We want to maximize the horizontal distance travelled by the projectile.

To do this, we find the launch angle θ_m that gives the maximum horizontal distance. The path function

$$p(\chi) = h + \chi tan\theta - \frac{g\chi^2}{2v^2}\sec^2\theta, \tag{5.1}$$

where $y = p(\chi)$ is the motion of projectile.

When the projectile hits the hill, there is a value of χ for which $P(\chi) = w(\chi)$ for each value of x. We wish to find the value of θ that maximizes x.

$$w(\chi) = p(\chi) = h + xtan\theta - \frac{g\chi^2}{2v^2}\sec^2\theta. \tag{5.2}$$

Differentiating (5.1) *implicitly with respect to θ, we have*

$$w'(\chi)\frac{d\chi}{d\theta} = \chi\sec^2\theta + \frac{d\chi}{d\theta}\tan\theta - \frac{g}{v^2}(\chi^2\sec^2\theta\tan\theta + \chi\frac{dx}{d\theta}\sec^2\theta). \tag{5.3}$$

Setting $\frac{dx}{d\theta} = 0$ in Eq (5.3)*, we have*

$$\chi_m = \frac{v^2}{g}\cot\theta_m \tag{5.4}$$

or

$$\theta_m = arctan(\frac{v^2}{g\chi_m}). \tag{5.5}$$

An enveloping parabola encloses and intersects all potential projectile paths. Henelsmith determined this parabola by maximizing the projectile height for a given horizontal distance, encompassing all possible paths.

Letting $w = \tan(\theta)$, in Eq (5.1)*, we get*

$$\psi = P(\chi) = h + \chi w - \frac{g\chi^2}{2v^2}(1 + w^2). \tag{5.6}$$

Differentiating (5.6) *with respect to w and setting $\psi' = 0$, we get, as Henelsmith obtained,*

$$\psi' = \chi - \frac{\chi g^2}{v^2}(w) = 0, \tag{5.7}$$

$$w = \frac{v^2}{g\chi}, \tag{5.8}$$

so that the enveloping parabola defined by

$$\psi_m = \rho(\chi) = h + \frac{v^2}{2g} - \frac{\chi g^2}{v^2}. \tag{5.9}$$

To solve the projectile problem, first determine the value of χ_m that makes the density function $\rho(\chi)$ equal to the function $w(\chi)$. Solving for θ_m in (5.5) *because we want to find the point at which the enveloping parabola ρ intersects the impact function w, and then find θ that corresponds to this point on the enveloping parabola. We choose a linear impact function $w(\chi) = 0.4x$ with h=10 and v=20. Let $g = 9.8$, then the nonlinear equation is given by,*

$$\Upsilon(\chi) = \rho(\chi) - w(\chi) = h + \frac{v^2}{2g} - \frac{g\chi^2}{2v^2} - 0.4\chi, \tag{5.10}$$

$\chi_0 = 30, \chi^* = 36.103018.$

The Table 1 summarizes the numerical results, showcasing the performance of both the proposed method and 16th-order method demonstrating its superiority. To further emphasize this point, the Figure 1 visually represents the error bounds for both methods. The reduction in error bounds signifies the enhanced accuracy and efficiency of our approach.

Table 1. Numerical comparison between proposed iterative method PM and 16th-order.

method	n	χ_n	$\mid \Upsilon(\chi_n) \mid$	$\mid \chi_{n-1} - \chi_n \mid$	COC	CPU Time
PM	1	36.103	4.1079×10^{-8}	3.19557×10^{-8}		
	2	36.103	0	0	10	0.125
16th YM	3	36.103	-	0	16.01	0.512152

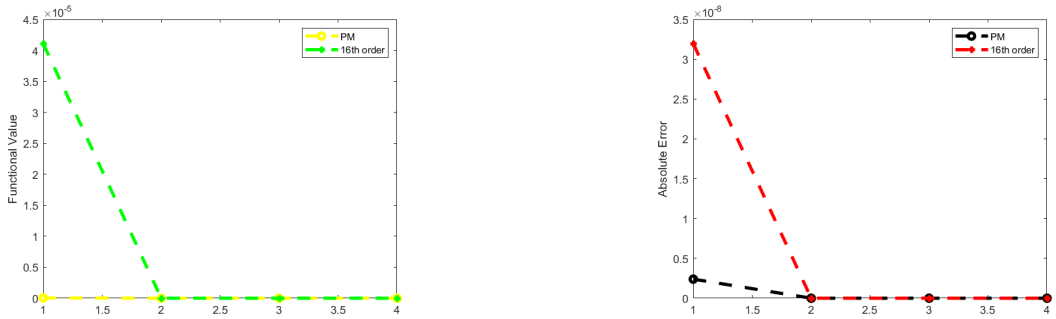

(a) $0.01225\chi^2 + 0.4\chi - 30.4082$(PM) **(b)** $0.01225\chi^2 + 0.4\chi - 30.4082$(16th YM)

Figure 1. Graphical comparison between proposed iterative method PM and 16th-order.

Example 5.2. *This problem is related to Plank's radiation law [2],*

$$\phi(t) = \frac{8\pi cht^{-5}}{e^{\frac{ch}{tkT}} - 1}.$$

Planck's radiation law is a formula used to calculate the energy density within a black body at

- *specific temperature= T;*
- *speed of light=c;*
- *wavelength =t;*
- *Planck's constant=h;*
- *Boltzmann's constant=k.*

By finding the maximum of the function $\phi(t)$ and its corresponding wavelength (t), one can use the derivative $\phi'(t) = 0$ to derive the maximum wavelength according to the law. This law is crucial in understanding the radiation emitted by black bodies at different temperatures. The maximum of the function $\phi(t)$ and the associated wavelength t can be derived from $\phi'(t) = 0$, and, therefore, by setting $\chi = \frac{ch}{tkT}$, we get the equation

$$e^{-\chi} + \frac{\chi}{5} - 1, (\chi_0 = 3).$$

Initial point $\chi_0 = 3$ will be used in the following numerical tests for finding the simple root $\alpha =$ 4.965114.

The Table 2 summarizes the numerical results, showcasing the performance of both the proposed method and 16th-order method demonstrating its superiority. To further emphasize this point, the Figure 2 visually represents the error bounds for both methods. The reduction in error bounds signifies the enhanced accuracy and efficiency of our approach.

Table 2. Numerical comparison between proposed iterative method PM and 16th-order.

method	n	χ_n	$\mid \Upsilon(\chi_n) \mid$	$\mid \chi_{n-1} - \chi_n \mid$	COC	CPU Time
PM	1	4.9651170871159177010	5.5×10^{-7}	2.9×10^{-6}		
	2	4.9651142317442763037	5.1×10^{-69}	2.6×10^{-68}	10	0.265
	3	4.9651142317442763037	2.4×10^{-689}	1.2×10^{-688}		
16th YM	1	4.9650723894771912524	8.1×10^{-6}	0.000042		
	2	4.9651142317442763037	9.2×10^{-51}	4.8×10^{-50}	16	0.828
	3	4.9651142317442763037	3.1×10^{-455}	1.6×10^{-454}		

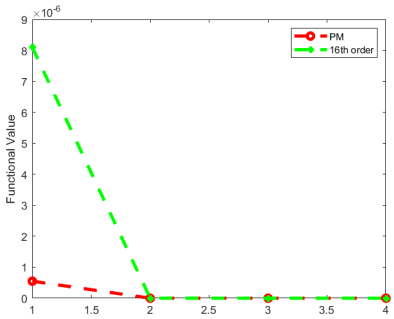

(a) $e^{-\chi} + \frac{\chi}{5} - 1$(PM)

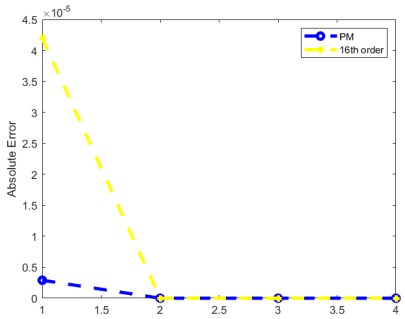

(b) $e^{-\chi} + \frac{\chi}{5} - 1$(16th YM)

Figure 2. Graphical comparison between proposed iterative method PM and 16th-order.

Example 5.3. *[12] Let $X = Y = C[0,1]$ represent the space of continuous functions defined on $[0,1]$, and both the spaces are equipped with the max-norm. Consider a subset of X denoted by Ω defined by $\Omega = \{\chi \in C[0,1]; \|\chi\| \leq R\}$, with $R > 1$, and Υ be defined on Ω by*

$$\Upsilon(\chi)(\varsigma) = \chi(\varsigma) - \Upsilon(\varsigma) - \mu \int_0^1 G(\varsigma, t)\chi(t)^3 dt, x \in C[0,1], \varsigma \in [0,1], \tag{5.11}$$

where, $\Upsilon \in C[0,1]$ is a given function, μ is a real constant, and the kernel G is the Green's function

$$G(\varsigma, t) = \begin{cases} (1-\varsigma)t, t \leq \varsigma, \\ (1-\varsigma)t, \varsigma \leq t. \end{cases} \tag{5.12}$$

In this case, for each $x \in \Omega$, $\Upsilon'(\chi)$ is a linear operator defined on Ω by the following expression:

$$\Upsilon'(\chi)(v)(\varsigma) = V(\varsigma) - 3\lambda \int_0^1 G(\varsigma, t)\chi(t)^2 v(t) dt, v \in C[0,1], \varsigma \in [0,1]. \tag{5.13}$$

By choosing, $\lambda_0 = 2.16, \lambda = 3.12, M = 1 + \lambda_0 t$*, then applying Theorem 4.1,* $r = \min\{r_1, r_2, r_3, r_4\} = 0.0155207$.

From the tabulated results in Table 3, the radius of convergence for our method suggests a wider range of initial conditions for which a solution exists and it provides numerical aspects of existence of solution. Hence, the solution exists in the region $U(\chi^*, 0.0155207)$.

Table 3. Radii of convergence.

λ_0	λ	M	r_1	r_2	r_3	r_4
2.16	3.12	$1 + \lambda_0 t$	0.268817	0.0699475	0.0454709	0.0155027

Example 5.4. *Let* $X = Y = R^3$, $\Omega = \overline{U}(0, 1)$*, [12] and*

$$x = \begin{pmatrix} 0 \\ 0 \\ 0 \end{pmatrix}. \tag{5.14}$$

Define the function F on Ω *for*

$$w = \begin{pmatrix} \chi \\ \psi \\ z \end{pmatrix}, \tag{5.15}$$

$$\Upsilon(w) = \begin{pmatrix} e^{\chi} \\ \frac{e-1}{2}\psi^2 + \psi \\ z \end{pmatrix}. \tag{5.16}$$

Then, the Fréchet-derivative is given by

$$\Upsilon'(v) = \begin{bmatrix} e^{\chi} & 0 & 0 \\ 0 & (e - \psi) + 1 & 0 \\ 0 & 0 & 1 \end{bmatrix}. \tag{5.17}$$

By choosing, $\lambda_0 = 2, \lambda = e, M = 1 + \lambda_0 t$*, then applying Theorem 4.1,* $r = \min\{r_1, r_2, r_3, r_4\} = 0.0183063$.

From the tabulated results in Table 4, the radius of convergence for our method suggests a wider range of initial conditions for which a solution exists and it provides snumerical aspects of existence of solution. Hence, the solution exists in the region $U(\chi^*, 0.0183063)$.

Table 4. Radii of convergence.

λ_0	λ	M	r_1	r_2	r_3	r_4
2	e	$1 + \lambda_0 t$	0.297695	0.0787637	0.0514214	0.0183063

Example 5.5. *Let* $X = [-1, 1]$, $Y = R$, $\chi_0 = 0$*, and let* $F : X \to Y$ *be the polynomial [12]*

$$\Upsilon(\chi) = \frac{\chi^3}{6} + \frac{\chi^2}{6} - \frac{5\chi}{6} + \frac{1}{9}. \tag{5.18}$$

By choosing, $\lambda_0 = \frac{13}{10}, \lambda = \frac{22}{10}, M = 1 + \lambda_0 t$*, then applying the Theorem 4.1,* $r = \min\{r_1, r_2, r_3, r_4\} = 0.0340465$.

From the tabulated results in Table 5, the radius of convergence for our method suggests a wider range of initial conditions for which a solution exists and it provides numerical aspects of existence of solution. Hence, the solution exists in the region $U(\chi^*, 0.0340465)$.

Table 5. Radii of convergence.

λ_0	λ	M	r_1	r_2	r_3	r_4
$\frac{13}{10}$	$\frac{22}{10}$	$1 + \lambda_0 t$	0.571429	0.121991	0.0753055	0.0340465

Example 5.6. *Let us consider an equation*

$$\chi^3 - 0.49 = 0. \tag{5.19}$$

Consider the domain $\Omega = U(\chi_0, 0.5)$*, where* $\chi_0 = 1$*. By choosing* $\lambda_0 = 2.5$*,* $\lambda = 3$*,* $M = 1 + \lambda_0 t$*, then applying Theorem 4.1,* $r = \min\{r_1, r_2, r_3, r_4\} = 0.510028$.

From the tabulated results in Table 6, the radius of convergence for our method suggests a wider range of initial conditions for which a solution exists and it provides numerical aspects of existence of solution. Hence, the solution exists in the region $U(\chi^*, 0.510028)$.

Table 6. Radii of convergence.

λ_0	λ	M	r_1	r_2	r_3	r_4
2.5	3	$1 + \lambda_0 t$	0.25	0.0684962	0.51078	0.510028

6. Basin of attraction

We focus here on the visual representation of the basins of attraction where $\Psi(\phi)$ is a predefined complex polynomial, written as $\phi(z)$, which is an important part of our proposed strategy. The concept of basins of attraction is fundamental in understanding the behaviour of iterative methods in complex dynamics. When ϕ^* represents a root of the function $\Psi(\phi)$, the basins of attraction for ϕ^* can be defined as the collection of all ϕ_0 values, such that initiating the method at ϕ_0 will ultimately converge to ϕ^*. Mathematically,

$$B(\phi^*) = \{z_0 \in \mathbb{C} : \phi(z) \to \phi^* \text{ as } n \to \infty\}. \tag{6.1}$$

The basins of attraction are able to be pictured as regions on a a complex plane. The complex polynomial $\phi(z)$ has several roots, and each one corresponds to a distinct basin. When we commence the iterative process from a particular starting point ϕ_0, it gravitates towards a root ϕ^* if it falls within the basin corresponding to that particular root.

Expanding the range of initial points across the complex plane allows for a more comprehensive analysis of the method's behavior. Even when the function's roots are real, a viable solution can be obtained. Illustrating the basins of attraction through figures proves to be an effective technique in understanding the method's behavior within the complex plane. Mathematica software is highly valuable for generating these visual representations. These have been discussed by many researchers.

Numerical approaches help understand complex dynamical systems by analyzing their behavior and exploring their outcomes based on foundational principles. It is crucial to examine each numerical method individually as they can yield differing results.

A complex polynomial of order n has n distinct roots, essentially the complex plane into "n" basins. However, the important thing is that these basins may not necessarily be uniformly distributed or even linked to each other.

Basin colouring is a technique for visualizing the regions created by complex polynomials. In this basin colouring , each of the distinct basins resulting from the polynomial's roots is assigned a unique color out of the total of "n" basins. By applying numerical methods, the initial points within a defined region or mesh are analyzed to determine which basin they converge to. The corresponding color is then applied to represent the specific basin. Varying color intensities indicate the number of iterations required for convergence to a root, i.e., converging faster shows with higher intensity. This coloring approach shows a meaningful geometric interpretations of nearly all types of complex polynomials.

The concept of a basin of attraction in the context of the complex approach is pioneered by Cayley. This section is dedicated to utilizing this graphical tool to visually represent the basins associated with our proposed method. Taking advantage of the computational capabilities of the Mathematica 11.3 software, we aim to illustrate the basins of attraction for complex functions. This approach enables a detailed and insightful exploration of the method's basin of attraction through a graphical representation of its convergence patterns.

In the complex plane, we take a rectangle denoted as $\Omega = [-3, 3] \times [-3, 3] \in \mathbb{C}$ consisting of a grid of 450 points along each axis. Employing our iterative methods, we initiate the process from every zero point $z^{(0)}$. With a cap of 100 iterations and a tolerance criterion of $|\phi(z^{(k)})| < 10^{-4}$, we ascertain whether $z^{(0)}$ is the basin of attraction for a particular zero or not. This determination is made if the iterative procedure leads to a zero of the polynomial within the defined tolerance. This systematic approach provides valuable insights into the basins of attraction associated with different zeros of the polynomial.

Problem 6.1. Let $\phi(z) = z(z^2 + 1)(z^2 + 4)$ having five zeros $\{0, i, -i, 2i, -2i\}$. In Figure 3 we carefully consider a rectangular area in the complex plane, denoted as $\Omega = [-3, 3] \times [-3, 3] \in \mathbb{C}$. Our approach involves initiating the iterative process from various points within this region. When the iterative technique fails to converge for a specific starting point z_0, we colored the point black. Conversely, points where convergence occurs are colorized. A convergence criterion of less than 10^{-4} guides us in determining when the convergence process is deemed complete. The interesting patterns and shapes formed by the edges of attraction areas is the Julia set. It serves to delineate the intricate structure of iteration functions and provides valuable insights into their behavior and convergence patterns. In Figure 3, the left side represents the basin of attraction for the proposed iterative method (10th PM), while the right side represents the basin of attraction for the 16th-order iterative method (16th YM).

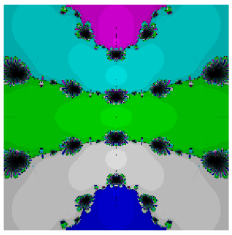

(a) $z(z^2 + 1)(z^2 + 4)$(PM)

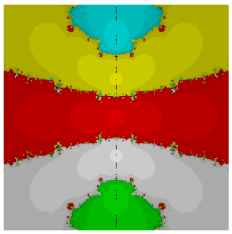

(b) $z(z^2 + 1)(z^2 + 4)$(16th YM)

Figure 3. Comparison of basins of attraction.

Problem 6.2. Let $\phi(z) = (z-1)^3 - 1$ [20] having three zeros $\{0.5 - 0.866025i, 0.5 + 0.866025i, 2\}$. In Figure 4, we carefully consider a rectangular area in the complex plane, denoted as $\Omega = [-3,3] \times [-3,3] \in \mathbb{C}$. Our approach involves initiating the iterative process from various points within this region. When the iterative technique fails to converge for a specific starting point z_0, we colored the point black. Conversely, points where convergence occurs are colorized. A convergence criterion of less than 10^{-4} guides us in determining when the convergence process is deemed complete. The interesting patterns and shapes formed by the edges of attraction areas is the Julia set. It serves to delineate the intricate structure of iteration functions and provides valuable insights into their behavior and convergence patterns. In Figure 4, the left side represents the basin of attraction for the proposed iterative method (10th PM), while the right side represents the basin of attraction for the 16th-order iterative method (16th YM).

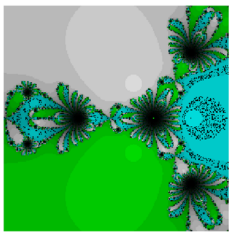

(a) $(z-1)^3 - 1$(PM)

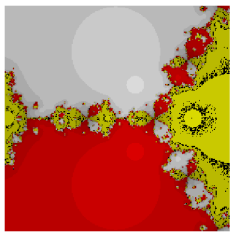

(b) $(z-1)^3 - 1$(16th YM)

Figure 4. Comparison of basins of attraction.

Problem 6.3. Let $\phi(z) = z^7 + 1$ having seven zeros $\{-0.62349 + 0.781831i, -0.62349 - 0.781831i, 0.22521 + 0.9749281i, 0.22521 - 0.9749281i, 0.900969 - 0.433884i, 0.900969 + 0.433884, -1\}$. In Figure 5, we carefully consider a rectangular area in the complex plane, denoted as $\Omega = [-3,3] \times [-3,3] \in \mathbb{C}$. Our approach involves initiating the iterative process from various points within this region. When the iterative technique fails to converge for a specific starting point z_0, we colored the point peach while in right side the technique fails to converge for a specific starting point z_0, we colored the point black . Conversely, points where convergence occurs are colorized. A convergence criterion of less than 10^{-4} guides us in determining when the convergence process is deemed complete. The interesting patterns and shapes formed by the edges of attraction areas is the Julia set. It serves to delineate the intricate structure of iteration functions and provides valuable insights into their behavior and convergence patterns. In Figure 5, the left side represents the basin of attraction for the proposed iterative method (10th PM), while the right side represents the basin of attraction for the 16th-order iterative method (16th YM).

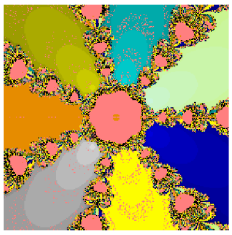

(a) $z^7 + 1$(PM)

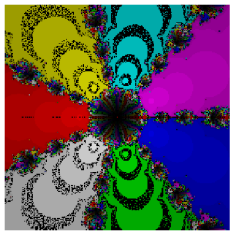

(b) $z^7 + 1$(16th YM)

Figure 5. Comparison of basins of attraction.

Problem 6.4. Let $\phi(z) = z^3 - z$ [21] having three zeros $\{-1, 0, 1\}$. In Figure 6, we carefully consider a rectangular area in the complex plane, denoted as $\Omega = [-3, 3] \times [-3, 3] \in \mathbb{C}$. Our approach involves initiating the iterative process from various points within this region. When the iterative technique fails to converge for a specific starting point z_0, we colored the point red. Conversely, points where convergence occurs are colorized. A convergence criterion of less than 10^{-4} guides us in determining when the convergence process is deemed complete. The interesting patterns and shapes formed by the edges of attraction areas is the Julia set. It serves to delineate the intricate structure of iteration functions and provides valuable insights into their behavior and convergence patterns. In Figure 6, the left side represents the basin of attraction for the proposed iterative method (10th PM), while the right side represents the basin of attraction for the 16th-order iterative method (16th YM).

(a) $z^3 - z$(PM) **(b)** $z^3 - z$(16th YM)

Figure 6. Comparison of basins of attraction.

Problem 6.5. Let $\phi(z) = z^4 - 5z^2 + 4$ [21] having four zeros $\{-2, -1, 1, 2\}$. In Figure 7, we carefully consider a rectangular area in the complex plane, denoted as $\Omega = [-3, 3] \times [-3, 3] \in \mathbb{C}$. Our approach involves initiating the iterative process from various points within this region. When the iterative technique fails to converge for a specific starting point z_0, we colored the point white. Conversely, points where convergence occurs are colorized. A convergence criterion of less than 10^{-4} guides us in determining when the convergence process is deemed complete. The interesting patterns and shapes formed by the edges of attraction areas is the Julia set. It serves to delineate the intricate structure of iteration functions and provides valuable insights into their behavior and convergence patterns. In Figure 7, the left side represents the basin of attraction for the proposed iterative method (10th PM), while the right side represents the basin of attraction for the 16th-order iterative method (16th YM).

(a) $z^4 - 5z^2 + 4$(PM) **(b)** $z^4 - 5z^2 + 4$(16th YM)

Figure 7. Comparison of basins of attraction.

Problem 6.6. Let $\phi(z) = z^7 - 1$ having seven zeros $\{0.62349 + 0.781831i, 0.62349 - 0.781831i, -0.22521 + 0.9749281i, -0.22521 - 0.9749281i, -0.900969 - 0.433884i, -0.900969 + 0.433884, 1\}$. In Figure 8, we carefully consider a rectangular area in the complex plane, denoted as $\Omega = [-3, 3] \times [-3, 3] \in \mathbb{C}$. Our approach involves initiating the iterative process from various points within this region. When the iterative technique fails to converge for a specific starting point z_0, we colored the point white. Conversely, points where convergence occurs are colorized. A convergence criterion of less than 10^{-4} guides us in determining when the convergence process is deemed complete. The interesting patterns and shapes formed by the edges of attraction areas is the Julia set. It serves to delineate the intricate structure of iteration functions and provides valuable insights into their behavior and convergence patterns. In Figure 8, the left side represents the basin of attraction for the proposed iterative method (10th PM), while the right side represents the basin of attraction for the 16th-order iterative method (16th YM).

(a) $z^7 - 1$(PM) **(b)** $z^7 - 1$(16th YM)

Figure 8. Comparison of basins of attraction.

Problem 6.7. Let $\phi(z) = (z^3 - i)(z + 2i)$ [10] having four zeros $\{-i, -2i, -0.866025 + 0.5i, 0.866025 + 0.5i\}$. In Figure 9, we carefully consider a rectangular area in the complex plane, denoted as $\Omega = [-3, 3] \times [-3, 3] \in \mathbb{C}$. Our approach involves initiating the iterative process from various points within this region. When the iterative technique fails to converge for a specific starting point z_0, we colored the point yellow. Conversely, points where convergence occurs are colorized. A convergence criterion of less than 10^{-4} guides us in determining when the convergence process is deemed complete. The interesting patterns and shapes formed by the edges of attraction areas is the Julia set. It serves to delineate the intricate structure of iteration functions and provides valuable insights into their behaviour and convergence patterns. In Figure 9, the left side represents the basin of attraction for the proposed iterative method (10th PM), while the right side represents the basin of attraction for the 16th-order iterative method (16th YM).

(a) $(z^3 - i)(z + 2i)$(PM) **(b)** $(z^3 - i)(z + 2i)$(16th YM)

Figure 9. Comparison of basins of attraction.

Problem 6.8. Let $\phi(z) = (z^2 - 1)(z^2 + 0.16)$ [10] having four zeros $\{-1, -0.4i, 0.4i, 1\}$. In Figure 10, we carefully consider a rectangular area in the complex plane, denoted as $\Omega = [-3, 3] \times [-3, 3] \in \mathbb{C}$. Our approach involves initiating the iterative process from various points within this region. When the iterative technique fails to converge for a specific starting point z_0, we colored the point light white shades. Conversely, points where convergence occurs are colorized. A convergence criterion of less than 10^{-4} guides us in determining when the convergence process is deemed complete. The interesting patterns and shapes formed by the edges of attraction areas is the Julia set. It serves to delineate the intricate structure of iteration functions and provides valuable insights into their behavior and convergence patterns.

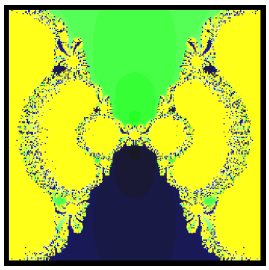

(a) $(z^2 - 1)(z^2 + 0.16)$(PM)

Figure 10. Comparison of basins of attraction.

Problem 6.9. Let $\phi(z) = (z^2+1)(z-1)^2$ [10] having zeros $\{-i, i, 1, 1\}$. In Figure 11, we carefully consider a rectangular area in the complex plane, denoted as $\Omega = [-3, 3] \times [-3, 3] \in \mathbb{C}$. Our approach involves initiating the iterative process from various points within this region. When the iterative technique fails to converge for a specific starting point z_0, we colored the point light white shades. Conversely, points where convergence occurs are colorized. A convergence criterion of less than 10^{-4} guides us in determining when the convergence process is deemed complete. The interesting patterns and shapes formed by the edges of attraction areas is the Julia set. It serves to delineate the intricate structure of iteration functions and provides valuable insights into their behavior and convergence patterns. In Figure 11, the left side represents the basin of attraction for the proposed iterative method (10th PM), while the right side represents the basin of attraction for the 16th-order iterative method (16th YM).

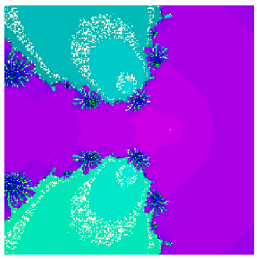

(a) $(z^2 + 1)(z - 1)^2$(PM)

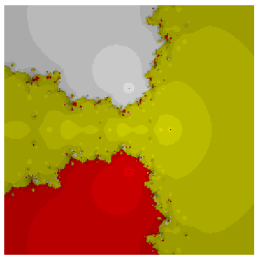

(b) $(z^2 + 1)(z - 1)^2$(16th YM)

Figure 11. Comparison of basins of attraction.

Problem 6.10. Let $\phi(z) = z^3 + z + 40$ having zeros $\{-3.32251, 1.66126 - 3.0462i, 1.66126 + 3.0462i\}$. In Figure 12, we carefully consider a rectangular area in the complex plane, denoted as $\Omega = [-3, 3] \times$

$[-3, 3] \in \mathbb{C}$. Our approach involves initiating the iterative process from various points within this region. When the iterative technique fails to converge for a specific starting point z_0, we colored the point black. Conversely, points where convergence occurs are colorized. A convergence criterion of less than 10^{-4} guides us in determining when the convergence process is deemed complete.The interesting patterns and shapes formed by the edges of attraction areas is the Julia set. It serves to delineate the intricate structure of iteration functions and provides valuable insights into their behavior and convergence patterns. In Figure 12, the left side represents the basin of attraction for the proposed iterative method (10th PM), while the right side represents the basin of attraction for the 16th-order iterative method (16th YM).

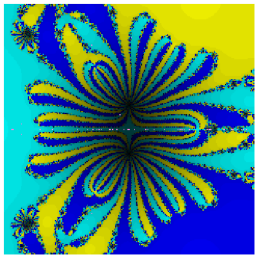

(a) $z^3 + z + 40$(PM)

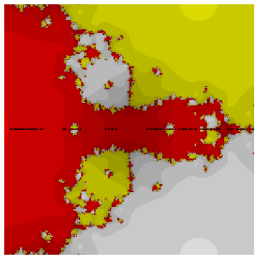

(b) $z^3 + z + 40$(16th YM)

Figure 12. Comparison of basins of attraction.

Problem 6.11. Let $\phi(z) = z^4 + 4z^3 - 24z^2 + 16z + 16$ having four zeros $\{2, 2, -7.4641, -0.535898\}$. In Figure 13, we carefully consider a rectangular area in the complex plane, denoted as $\Omega = [-3, 3] \times [-3, 3] \in \mathbb{C}$. Our approach involves initiating the iterative process from various points within this region. When the iterative technique fails to converge for a specific starting point z_0, we colored the point white. Conversely, points where convergence occurs are colorized. A convergence criterion of less than 10^{-4} guides us in determining when the convergence process is deemed complete. The interesting patterns and shapes formed by the edges of attraction areas is the Julia set. It serves to delineate the intricate structure of iteration functions and provides valuable insights into their behavior and convergence patterns. In Figure 13, the left side represents the basin of attraction for the proposed iterative method (10th PM), while the right side represents the basin of attraction for the 16th-order iterative method (16th YM).

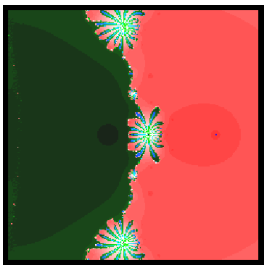

(a) $z^4 + 4z^3 - 24z^2 + 16z + 16$(PM)

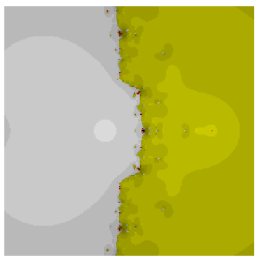

(b) $z^4 + 4z^3 - 24z^2 + 16z + 16$(16th YM)

Figure 13. Comparison of basins of attraction.

7. Conclusions

In this research article, we embarked on a journey to explore and develop 10th-order iterative methods for the solution of nonlinear equations with efficiency index 1.4677992. By employing the Frechet derivative of the first order, we established a foundation for achieving local convergence. This mathematical framework allowed us to tailor our iterative methods to exhibit efficient and reliable convergence behavior within specific regions, enhancing the applicability of our approach to a diverse array of nonlinear problems. The basin of attraction not only provides insights into the reliability of our methods, but also enables practitioners to strategically select starting points that expedite convergence. The results of our research not only contribute to the theoretical understanding of iterative methods, but also offer practical tools for solving nonlinear equations encountered in various scientific and engineering domains.

Use of AI tools declaration

The authors declare they have not used Artificial Intelligence (AI) tools in the creation of this article.

Conflict of interest

The authors do not have any conflict of interest.

References

1. A. Cordero, J. A. Ezquerro, M. A. Hernández-Verón, J. R. Torregrosa, On the local convergence of a fifth-order iterative method in Banach spaces, *Appl. Math. Comput.*, **251** (2015), 396–403. https://doi.org/10.1016/j.amc.2014.11.084
2. Y. Tao, K. Madhu, Optimal fourth, eighth and sixteenth order methods by using divided difference techniques and their basins of attraction and its application, *Mathematics*, **7** (2019), 322. https://doi.org/10.3390/math7040322
3. I. K. Argyros, S. K. Khattri, S. George, Local convergence of an at least sixth-order method in Banach spaces, *J. Fixed Point Theory Appl.*, **21** (2019), 23. https://doi.org/10.1007/s11784-019-0662-6
4. S. Amat, I. K. Argyros, S. Busquier, M. A. Hernández-Verón, E. Martínez, On the local convergence study for an efficient k-step iterative method, *J. Comput. Appl. Math.*, **343** (2018), 753–761. https://doi.org/10.1016/j.cam.2018.02.028
5. T. M. Pavkov, V. G. Kabadzhov, I. K. Ivanov, S. I. Ivanov, Local convergence analysis of a one parameter family of simultaneous methods with applications to real-world problems, *Algorithms*, **16** (2023), 103. https://doi.org/10.3390/a16020103
6. P. Maroju, Á. A. Magreñán, Í. Sarría, A. Kumar, Local convergence of fourth and fifth order parametric family of iterative methods in Banach spaces, *J. Math. Chem.*, **58** (2020), 686–705. https://doi.org/10.1007/s10910-019-01097-y

7. A. Kumar, P. Maroju, R. Behl, D. K. Gupta, S. S. Motsa, A family of higher order iterations free from second derivative for nonlinear equations in R, *J. Comput. Appl. Math.*, **330** (2018), 676–694. https://doi.org/10.1016/j.cam.2017.07.005
8. F. Soleimani, F. Soleymani, S. Shateyi, Some iterative methods free from derivatives and their basins of attraction for nonlinear equations, *Discrete Dyn. Nat. Soc.*, **2013** (2013), 301718. https://doi.org/10.1155/2013/301718
9. S. Singh, D. K. Gupta, Iterative methods of higher order for nonlinear equations, *Vietnam J. Math.*, **44** (2016), 387–398. https://link.springer.com/article/10.1007/s10013-015-0135-1
10. S. Sutherland, *Finding roots of complex polynomials with Newton's method*, Boston University, 1989.
11. H. Singh, J. R. Sharma, Simple yet highly efficient numerical techniques for systems of nonlinear equations, *Comput. Appl. Math.*, **42** (2023), 22. https://doi.org/10.1007/s40314-022-02159-9
12. A. A. Magreñán-Ruiz, I. K. Argyros, Two-step Newton methods, *J. Complexity*, **30** (2014), 533–553. https://doi.org/10.1016/j.jco.2013.10.002
13. G. A. Nadeem, W. Aslam, F. Ali, An optimal fourth-order second derivative free iterative method for nonlinear scientific equations, *Kuwait J. Sci.*, **50** (2023), 1–15. https://doi.org/10.48129/kjs.18253
14. P. Maroju, R. Behl, S. S. Motsa, Some novel and optimal families of King's method with eighth and sixteenth-order of convergence, *J. Comput. Appl. Math.*, **318** (2017), 136–148. https://doi.org/10.1016/j.cam.2016.11.018
15. A. K. Maheshwari, A fourth order iterative method for solving nonlinear equations, *Appl. Math. Comput.*, **211** (2009), 383–391. https://doi.org/10.1016/j.amc.2009.01.047
16. V. Arroy, A. Cordero, J. R. Torregrosa, M. P. Vassileva, Artificial satellites preliminary orbit determination by the modified high-order Gauss method, *Int. J. Comput. Math.*, **89** (2012), 347–356. https://doi.org/10.1080/00207160.2011.560266
17. N. Y. Abdul-Hassan, A. H. Ali, C. Park, A new fifth-order iterative method free from second derivative for solving nonlinear equations, *J. Appl. Math. Comput.*, **68** (2022), 2877–2886. https://doi.org/10.1007/s12190-021-01647-1
18. A. S. Alshomrani, R. Behl, P. Maroju, Local convergence of parameter based method with six and eighth order of convergence, *J. Math. Chem.*, **58** (2020), 841–853. https://doi.org/10.1007/s10910-020-01113-6
19. O. S. Solaiman, I. Hashim, Two new efficient sixth order iterative methods for solving nonlinear equations, *J. King Saud Univ. Sci.*, **31** (2019), 701–705, https://doi.org/10.1016/j.jksus.2018.03.021
20. R. Behl, P. Maroju, S. S. Motsa, A family of second derivative free fourth order continuation method for solving nonlinear equations, *J. Comput. Appl. Math.*, **318** (2017), 38–46. https://doi.org/10.1016/j.cam.2016.12.008
21. A. G. Wiersma, *The complex dynamics of Newton's method*, University of Groningen, 2016.

AIMS Press